Icarus 255 (2015) 51–57

Contents lists available at ScienceDirect

Icarus

journal homepage: www.elsevier.com/locate/icarus

The lunar surface-exosphere connection: Measurement of secondary-ions from Apollo soils

C.A. Dukes *, R.A. Baragiola

University of Virginia, Laboratory for Atomic and Surface Physics, Charlottesville, VA 22904, USA

ARTICLE INFO

Article history:
Received 15 August 2014
Revised 18 October 2014
Accepted 24 November 2014
Available online 4 December 2014

Keywords:
Ionospheres
Abundances, atmospheres
Moon, surface
Moon
Regoliths

ABSTRACT

Low energy secondary ions ejected by the solar wind are an important component of tenuous exospheres surrounding airless bodies, since these ions carry information on the planetary surface composition. In this work we examine the dependence of secondary-ion abundance, as a function of energy and mass, on surface composition. The surface compositions of two Apollo soils (10084 and 62231) and a synthetic Corning glass lunar simulant were measured with X-ray photoelectron spectroscopy and correlated with the spectra of secondary-ions ejected from the same soils by 4 keV He ions. XPS spectra for lunar soils show that the surface compositions are similar to the bulk, but enriched in Fe and O, while depleted in Mg and Ca. 4 keV He irradiation on the lunar soils and a glass simulant preferentially removes O and Si, enriching the surface in Al, Ti, Mg, and Ca. Secondary-ion species ejected from the Apollo soils by 4 keV He include: Na^+, Mg^+, Al^+, Si^+, Ca^+, Ca^{++}, Ti^+, Fe^+, and molecular species: NaO^+, MgO^+ and SiO^+. Secondary ion energy distributions for lunar soil 10084 and 62231 rise rapidly, reach a maxima at ~5 eV for molecular ions and Na^+, ~7.5 eV for Fe^+, and ~10 eV for Mg^+, Al^+, Si^+, Ca^+ and Ti^+, then decrease slowly with energy. We present species-dependent relative conversion factors for the derivation of atomic surface composition from secondary-ion count rates for 4 keV He irradiation of lunar soils 10084 and 62231, as well as the Corning glass lunar simulant.

1. Introduction

The abundance of low energy ions in the tenuous atmospheres near the surface of airless planetary bodies such as the Moon, Mercury, and asteroids should be largely indicative of the planetary surface elemental composition (Johnson and Baragiola, 1991). This is due to the negligible interaction of sputtered particles with other species in an exosphere. For the Moon, the exosphere is defined as the region of space bounded by the lunar surface and reaching an altitude of ~100 km. The atomic density of is so low, $<10^6$ cm^{-3}, that no physical or chemical interaction can occur between particles which are retained in the lunar envelope by gravity or lost to space, depending on velocity and trajectory. The lunar exosphere is composed primarily of species from the lunar surface: neutrals atoms desorbed by solar photons (PSD) and electrons (ESD), sputtered by solar wind ions, thermally desorbed, ejected during meteoritic impact, and derived from radioactive decay. At this time (prior to LADEE) definitive observations of neutral atoms in the lunar exosphere have been limited to Ar, He, H_2, K, Na, O, ^{210}Po and ^{222}Rn (Hodges, 1973; Hoffman et al., 1973; Potter and Morgan, 1988; Vorburger et al., 2014; Bjorkholm et al., 1973; Gorenstein and Bjorkholm, 1973; Lawson et al., 2005). Recent observations by the Lunar Reconnaissance Orbiter's Lyman-Alpha Mapping Project (LAMP) confirmed the presence of He (Stern et al., 2012; Feldman et al., 2012) and H_2 in the lunar exosphere (Stern et al., 2013), while Chandrayaan-1's Energetic Neutral Analyzer (CENA) has reported the first observation of neutral O, presumably sputtered from the lunar surface by the solar wind (Vorburger et al., 2014).

The ionic component of the lunar exosphere is derived from a number of processes: photo-ionization of sputtered or desorbed neutral atoms, solar wind primary ions, and secondary ions generated from solar wind impact. The sputtered ion species are important, as their abundance reflects the lunar surface composition. In addition, sputtered ions may also continue to interact with the lunar surface by charging or neutralizing regions of the regolith and by self-sputtering (Poppe et al., 2013). These ions can be observed locally by mass spectrometers that allow the identification of charged exospheric components. Measurements from AMPTE, WIND, and SELENE have identified Ar^+, Na^+, K^+, Si^+, Al^+, C^+, and O^+ plus solar wind ions (Hilchenbach et al., 1993; Stern, 1999; Yokota et al., 2009, 2014). Recent measurements by LADEE of the lunar ion component are expected to add to this list.

* Corresponding author.
E-mail address: cdukes@virginia.edu (C.A. Dukes).

http://dx.doi.org/10.1016/j.icarus.2014.11.032
0019-1035/

Secondary ion/atom emission by sputtering is a physical process which occurs when energetic (>20 eV) primary ions impact atoms on a surface, transferring energy and momentum such that one (or more) of the surface atoms or molecules are ejected. In the laboratory, mass analysis of secondary ions (positive or negative) ejected by incident energetic (∼keV) ions is termed secondary ion mass spectroscopy (SIMS) and is often used to infer surface specific composition. Since secondary ion intensities (ion yields) cannot be simply matched directly to surface composition, but are dependent on primary ion type, atom ionization potential, and the local sample matrix, it is common to use calibration standards of known composition that closely match the sample of interest to enhance the quantitative information that can be extracted from SIMS.

Positive SIMS spectra for keV H^+, He^+, Ne^+ and Ar^+ impact on lunar soil *simulants* confirm that many ion species, beyond those identified in the lunar atmosphere, are ejected at significant fluxes and may exist in the lunar exosphere (Elphic et al., 1991). Simulants, however, have very different surface characteristics than lunar soils, which contain grains of different morphology and composition, as many lunar grains have vapor deposited and radiation altered rims. To relate secondary ion emission to surface composition of Apollo soils, we performed experiments using 4 keV He^+ on two mature lunar soils where we measured secondary ion mass and energy spectra and correlated to XPS measurements of elemental surface composition in ultrahigh vacuum (UHV).

2. Experimental procedure

For this study, two mature lunar soils, Apollo 16 highland 62231 (I_s/FeO = 91) and Apollo 11 mare 10084 (I_s/FeO = 78), were irradiated with 4 keV He^+ in a UHV chamber (<10^{-9} Torr) at room temperature (∼295 K). The entire allocated lunar soil size fraction (<1 mm) was used without further sieving in order to provide a particle size distribution analogous to the lunar surface. We note that optical and electron microscope images of the samples show that the larger lunar grains are loosely coated with much smaller grains (<10 μm), enhancing the small size grain fraction in the SIMS and XPS analyses. Highland 62231 soil, collected from the rim of Buster Crater, is compositionally typical of the analyzed highland soils, with a Al_2O_3:FeO ratio falling toward the high end of the distribution. Mare 10084, a fine-grained basaltic soil with agglutinate and glassy inclusions, lies in the low Al_2O_3:FeO range of the standard mare compositional range for lunar soils. Lunar soil samples were prepared by sprinkling uncompacted soil onto UHV-compatible double-sided carbon tape fixed to a Cu mount. Good coverage (>98%) of the carbon tape was ensured by multiple successive coating of soil onto the tape and subsequent observation under an optical microscope.

A Physical Electronics Inc. (PHI) 04-303 ion gun, with an electron bombardment source, is mounted on the mu-metal lined analysis chamber and directed ions toward the sample at 42° from the sample normal (Fig. 1). However, since the soil surface is topographically irregular, local impact and collection angles varied. Ions were rastered 6 × 6 mm^2 across the sample surface to cover the entire ion mass-spectrometer entrance aperture, as well as to ensure uniform irradiation across the entire XPS analysis area. Total primary beam current, measured on the sample without bias, was ∼4 μA.

Secondary ions, ejected from the outermost 1–2 monolayers (∼6 Å) of the sample by the 4 keV primary He ions, were collected at 60° from the sample normal (in the forward direction) and measured by a Hiden Analytical EQS mass spectrometer equipped with a high-transmission 45-degree sector-field ion-energy analyzer (Fig. 1). For this study, positive SIMS spectra were measured at

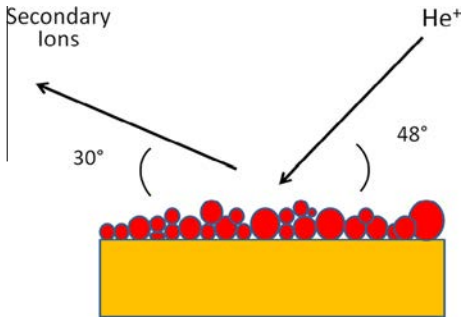

Fig. 1. Experimental geometry for secondary ion mass spectrometry with 4 keV He ions. Surface composition (∼5 nm) for the same sample region is obtained *in situ* by X-ray photoelectron spectroscopy.

ejected ion energies from 2 to 36 eV, a range where the instrument transmission is expected to be constant as a function of energy. However, quadrupole transmission does vary inversely with mass, passing light mass ions more readily (i.e. Batey, 1987), and requires a correction for absolute measurements. These corrections are not included in the raw spectra presented. The extraction lens voltages were optimized for ions of Mass 27 (Al^+) before collecting spectra. Because the lunar soils charged significantly under ion bombardment, the sample surface was charge neutralized during SIMS data collection using low energy (⩽4 eV) electrons. Secondary ion mass spectra were obtained from 0.4 to 100 amu, at a resolution of 0.1 amu. Each spectrum was taken in less than 10 min, and averaged over 10 cycles. Secondary ion energy spectra were collected at masses: 23 (Na^+), 24 (Mg^+), 27 (Al^+), 28 (Si^+), 40 (Ca^+ or MgO^+), 48 (Ti^+), 56 (Fe^+), and 39 (NaO^+ or K^+) amu from 0 to 100 eV in steps of 0.2 eV, at a 0.5 s dwell time and averaged over 8 cycles. Surface charge neutrality was maintained with the electron flood gun.

The secondary ion flux was compared with the surface elemental composition of the samples, measured *in situ* using X-ray photoelectron spectroscopy (XPS). This technique provides compositional information from the outermost surface (∼1–5 monolayers) of a sample. While the XPS depth sensitivity is slightly less than that for secondary ions, both techniques sample the surface region of the vapor-deposited rims (∼60–100 nm) surrounding most lunar grains (Keller and McKay, 1997). By comparing the intensities of the photoelectron peaks, adjusted with empirical instrumental sensitivity factors (Wagner, 1983), the elemental atomic concentrations can be determined with a sensitivity of ∼0.1% (atomic percent). Al X-rays (1486.6 eV) eject photoelectrons from sample atoms; their kinetic energy is measured using a PHI 560 double-pass cylindrical electron-energy analyzer (CMA) (Dukes et al., 1999; Loeffler et al., 2008). The spectrometer was operated at a fixed pass energy: 200 eV for survey spectra and 50 eV for high-resolution spectra, providing an instrument energy resolution of 3.2 eV and 0.8 eV, respectively. The measured kinetic energy of the photoelectron is given by the atomic binding energy of the electron, the X-ray energy and the spectrometer work function as: KE = γ − BE − φ_s. Determination of electron binding energy provides both atom identification and chemical bonding information. During the measurements, the electron flood gun was used to suppress positive surface charge due to photoelectron emission. The flood gun parameters employed for XPS measurement were identical to those used for the corresponding secondary ion energy spectra. For all samples XPS analysis was done before and after He^+ irradiation.

To calibrate the measurement of secondary ion intensity using the Hiden EQS quadrupole, we use two standards: a Corning glass lunar simulant section and synthetic forsterite powder. The synthetic lunar glass simulant, designed for NASA's Johnson Space

Center by Corning, is a reasonable calibration standard with high homogeneity and a bulk elemental composition similar to basaltic lunar soil (Eick et al., 1996). The stoichiometry of the glass simulant is similar to the lunar soils 10084 and 62231, excluding the Na or K content. The absolute surface concentrations of these alkalis are notoriously unreliable, since these cations are particularly mobile, diffusing in and out of the surface region in response to surface electric fields (Dukes et al., 2011; Magee and Harrington, 1978). In our analysis, we attempt to control for a changing surface concentration by short data acquisition intervals and XPS measurements before and after irradiation. SIMS data were taken in random order of secondary ion energy to decouple the effect of sputter reduction of surface Na from any potential secondary ion energy dependence.

3. Results

As methodology confirmation, we measured the surface composition and secondary ion spectra of a Corning Glass Works lunar simulant of known composition. Neglecting the carbon due to atmospheric contamination, XPS analysis shows a *surface* within 20% of measured *bulk* composition as determined by electron microprobe (Eick et al., 1996). The constituents and their relative weights are given in Table 1. We find enrichments of O and Al at the surface. However, XPS spectra of the glass after 4 keV He^+ irradiation and immediately subsequent to SIMS acquisition show a notable change in surface composition, with O and Si preferentially removed. Thus, we use the glass composition measured immediately after SIMS analysis to compare with the secondary ion emission spectra (Table 1). This composition is: 62.7% O, 13.3% Si, 9.3% Al, 5.5% Ca, 3.7% Fe, 3.4% Mg, and 2.1% Ti as derived from Fig. 2a.

Mass spectra for positive secondary ions ejected by 4 keV He^+ from the glass simulant were collected for secondary ion energies: 6, 10, 14, 18, and 24 eV. A mass spectrum for 10 eV secondary ions shows Ca^+ (MgO^+), Ca^{++}, Mg^+, Al^+, Si^+, Ti^+, Fe^+, and Na^+ ions, along with their isotopes in the appropriate concentration (Fig. 2b). To a large extent, the relative concentrations of these ions match the surface composition of the glass simulant, with the addition of Na, which is measured to a level below 0.1% with XPS, and without O, which is primarily sputtered as a neutral atom or negative ion. While spectra were taken from 0.4 to 100 amu, no species were observed below 20 amu or above 57 amu, and secondary ion spectra are shown in an abbreviated region (Fig. 2b). The secondary ion peak at 40 amu is a convolution derived from both Ca^+ and MgO^+ ions, as MgO^+ ejection was observed during 4 keV He irradiation of synthetic forsterite (which contains no Ca). However, the relative intensity of the MgO^+ to Mg^+ secondary ion peaks was only ~4% in forsterite (Fig. 3), thus we assume the secondary ion peak at 40 amu for all spectra is primarily due to Ca^+. No O^+ or H_3O^+ were observed in any positive secondary ion spectra. Spectra acquired at differing secondary ion energies show that while the spectral components are identical, their relative intensity ratios are not, due to the different secondary ion energy distributions for each species. In addition, for the lunar glass simulant, the secondary ion yields increased linearly with secondary ion energy for 2–14 eV, reaching a plateau at 14–24 eV. Spectra at differing secondary ion energies were taken by adjusting the voltage of the extraction lens and the pass energy of the quadrupole. Transmission through the Hiden SIMS instrument is independent of energy in the examined energy range (Hiden Anal., personal communication).

For synthetic forsterite, 6.5 eV secondary ion count rates and XPS spectra were measured as a function of fluence. There is a long term effect of ion irradiation on the ejection of secondary ions from forsterite. The SIMS spectrum is not constant with fluence as surface contaminant Na is removed; the secondary ion ejecta composition reaches equilibrium after $\sim 4 \times 10^{17}$ He^+ cm^{-2} (Fig. 3). XPS suggests that a trace amount of Na exists on the forsterite surface prior to ion irradiation, which is reduced below the sensitivity of the XPS instrument after 4 keV He irradiation. Since SIMS is more sensitive than XPS, it reveals Na and NaO signals that are seen to degrade with fluence, but remain detectable after 7.1×10^{17} He^+ cm^{-2} (Fig. 3).

We measured the secondary ion mass spectrum (10 eV ions) of the lunar highland soil 62231 (Fig. 4) and compared with XPS spectra (Fig. 4b and d). Ca^+ (MgO^+), Ca^{++}, Mg^+, Al^+, Si^+, SiO^+, Fe^+ (CaO^+), Na^+, and NaO^+ ions were consistently observed, along with their associated isotopes in the appropriate concentration (Table 1). The peak at 39 amu is identified as NaO^+, rather than K^+, for several reasons. First, no K is evident in the XPS spectra, nor measured by Korotev (1982). Second, while Sheffer (2007) does observe K in electron microprobe studies of soil 62231, it is at a level 20% of Na, inconsistent with the secondary ion ratio (1 ± 0.2) for Mass 23 to Mass 39 in our spectra. Thirdly, if we assume that the peak at Mass 39 is a mixture of K^+ and NaO^+, we expect analogously to observe KO^+, however, no peak is apparent above background at Mass 55. Finally, no asymmetry or increased width is apparent in the peak at Mass 39. Thus, any contribution from K^+ is negligible for the purposes of this study. A similar argument can be made for the identification of Mass 39 in the mare soil.

No O^+ was detected from soil 62231, indeed no secondary ions were observed below 20 amu or above 63 amu. The carbon signal is excluded in the XPS analysis, since it was assumed to be terrestrial in origin, stemming from adventitious carbon and/or from small exposed areas of the carbon tape. We note that the surface composition, which can vary from bulk composition due to surface segregation and diffusion of species, is consistent with the published bulk composition for highland soil 62231 (Sheffer, 2007; Korotev, 1982) (Table 1) and adjacent lunar soil sample 62241 (Korotev, 1981). Total spectral count rates for the highland (and mare) soil are maximal for secondary ion energies around 14 eV. Alkalis are ejected as ions at higher rates than elements of comparable surface concentration, due to their low ionization potential, which enhances their signal intensity relative to other species. In addition, we find the count rate for higher mass ions is enhanced by collecting secondary ions with greater energy.

Identical measurements of surface composition and secondary ion emission were made for lunar mare soil 10084 (Fig. 4a and c). XPS analysis provides a surface composition (Table 1) consistent with the measured soil bulk composition (Korotev and Gillies, 2001). Secondary ion mass spectra from the mare soil reflect the higher Ti content and lower feldspar concentration of this material when compared with highland 62231, with increased Mg^+ and Fe^+ signals relative to Na^+ and Ca^+ (Fig. 4). No secondary ions with mass below 20 amu, including O^+, or above 63 amu were observed.

Energy distributions for secondary ions ejected by 4 keV He^+ were measured for the Corning glass lunar simulant, forsterite, highland soil 62231, and mare soil 10084. Typical of secondary ions ejected from insulating surfaces, the distributions all rise rapidly, peak below 15 eV, and then drop off slowly with energy. Secondary ion energy distributions for lunar soil 10084 (Fig. 5) and 62231 (Fig. 6) vary with soil and ion type—the maxima of the distributions are at 5 eV for molecular ions and Na^+, ~7.5 eV for Fe^+, and ~10 eV for Mg^+, Al^+, Si^+, Ca^+ and Ti^+.

4. Discussion

XPS analyses of the pristine lunar soil show a surface enrichment of O and Fe and depletions of Mg and Ca relative to the bulk composition for both 10084 and 62231. The magnitude of the

Table 1
Composition of lunar soils 10084, 62231 and Corning lunar glass simulant (atomic%) and secondary ion count rate for 4 keV He^+ (I = 4 μA). Composition of lunar soils 10084, 62231 and Corning lunar glass simulant (atomic%) and secondary ion count rate for Korotev and Gillies (2001). Atomic percent values for bulk 62231 are derived from the oxide values forthe <45 micron size fraction measured by Sheffer (2007) and from Eick et al. (1996) for Corning glass lunar simulant. The simulant bulk composition also includes 0.1 atomic% Cr. Surface (unirradiated) and irradiated (>4 × 10^{17} He^+ cm^{-2} irradiation) atomic concentrations are measured by XPS.

	10084				62231				Corning glass lunar simulant			
	Bulk (atom%)	Surface (atom%)	Irrad (atom%)	Sec. ions (cps)	Bulk (atom%)	Surface (atom%)	Irrad (atom%)	Sec. ions (cps)	Bulk (atom%)	Surface (atom%)	Irrad (atom%)	Sec. ions (cps)
Si	16.1	15.8	15.1	164	16.3	18.4	14.2	94	18.2	15.5	13.3	139
Al	6.1	7.0	8.4	368	11.3	9.6	13.1	258	5.8	8.0	9.3	344
Ti	2.2	0.8	1.7	57	0.2	0.1	0.2	8	1.9	1.7	2.1	53
Fe	5.1	6.1	5.0	69	1.5	2.3	1.9	36	4.1	3.4	3.7	58
Mg	4.5	1.2	4.2	154	3.4	0.7	2.5	85	3.9	2.3	3.4	214
Ca	4.9	2.2	5.3	252	6.0	3.1	5.3	155	4.2	4.5	5.5	327
Na	0.3	0.2	0.8	38	0.3	0.2	0.3	54	<0.1	<0.1	<0.1	<1
K	0.1	<0.1	<0.1	<0.1	0.1	<0.1	<0.1	<0.1	<0.1	<0.1	<0.1	<1
Mn	0.1	0.3	0.3	<0.1	<0.1	<0.1	<0.1	<0.1	0.1	<0.1	<0.1	<1
P	<0.1	<0.1	<0.1	<0.1	<0.1	<0.1	<0.1	<0.1	<0.1	<0.1	<0.1	<1
O	60.6	66.4	59.1	<0.1	61.0	65.5	62.5	<0.1	61.6	64.6	62.7	<1

enrichment or depletion is sample dependent. These findings are consistent with previous studies of 10084 by Baron et al. (1977), who reviewed published XPS and AES measurements and found Fe enrichment at the surface, relative to the bulk concentration, as well as Mg, Ca, and Al depletion for lunar mare 10084 and Fra Mauro soil 14003. Similarly, we find a 15% surface depletion of Al for 62231, but observe a 15% enhancement of Al for 10084 at the surface. However, since the surfaces of all measured lunar soils have been exposed to varying degrees of contamination from the Earth's atmosphere or sample preparation, small differences in surface composition should not be overemphasized.

Ion irradiated soils are better matched to the pristine lunar environment, since daytime solar wind irradiation is continual

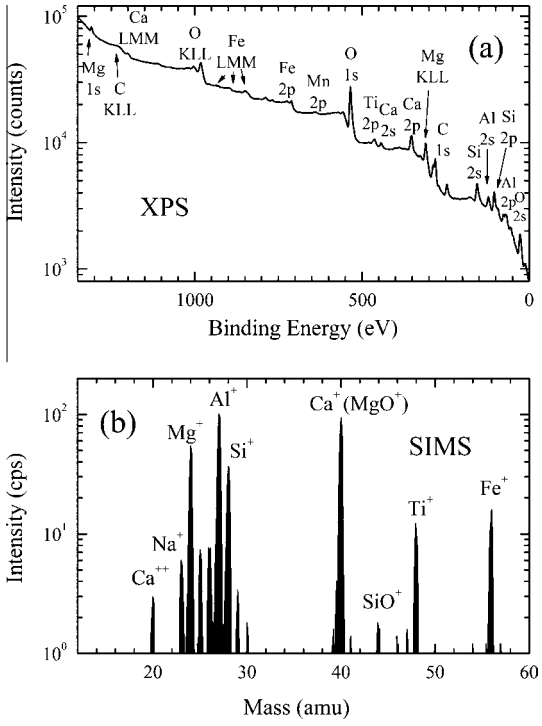

Fig. 2. Corning glass lunar simulant was used to calibrate secondary ion mass spectra to surface composition. (a) The Al Kα XPS spectrum of the glass surface (topmost ~5 nm) was determined after SIMS measurements. (b) Secondary ion mass spectrum of 10 eV ions emitted from the identical surface by 4 keV He^+ primary ions. Additional ion peaks are isotopes of the identified primary peaks.

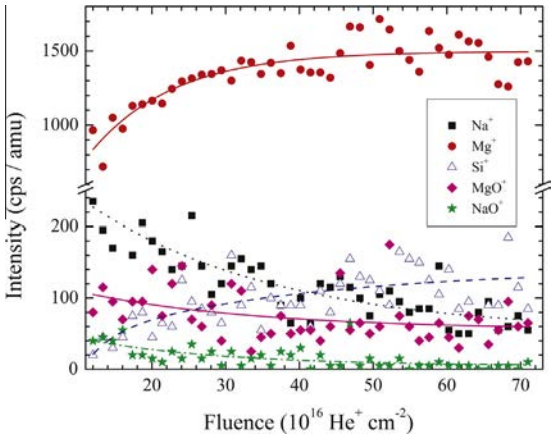

Fig. 3. The long-term effect of 4 keV He^+ irradiation on secondary ion emission from synthetic forsterite (Mg_2SiO_4) shows that Mg^+ and Si^+ increase with fluence to an equilibrium, as Na impurities at the surface and surface oxides are depleted. After a fluence of ~4 × 10^{17} He^+ cm^{-2}, the secondary ion emission reaches an equilibrium intensity beyond which the composition of the ion ejecta does not change.

across the surface of the Moon. In addition, ion sputtering removes atmospheric surface contaminants and forms an amorphous region to the ion penetration depth, similar to the rims observed on lunar grains (Keller and McKay, 1997). Hence, we use the XPS surface compositional measurements of irradiated soil collected immediately after secondary ion collection as a proxy for the *in situ* lunar regolith to correlate to the secondary ion emission spectra. The effect of sputtering by 1 keV/amu ions is well known (i.e. Dukes et al., 1999; Hapke, 2001; Loeffler et al., 2008), removing oxygen from the surface and chemically reducing iron in minerals and lunar material. This data set (Table 1) shows similar chemical reduction in lunar soil and simulant after ion irradiation, with O preferentially removed along with Si, which is sputtered at a slower rate. This is consistent with observed Si enrichments in Ar^+ irradiated SiO_2 (Betz and Wehner, 1983). Ion irradiation increases the relative surface concentrations of Al, Ti, Ca, and Mg in both 10084 and 62231, as well as in the glass simulant. Thus, an enrichment of these elements in lunar grains rims, relative to the bulk is expected. Keller and McKay (1997) describe the composition of lunar soil grain rims and find that Fe and Ti are the only constituents that consistently enrich the grain rim, concluding that these rims must be formed by a combination of processes, rather than just solar wind irradiation damage. These processes include

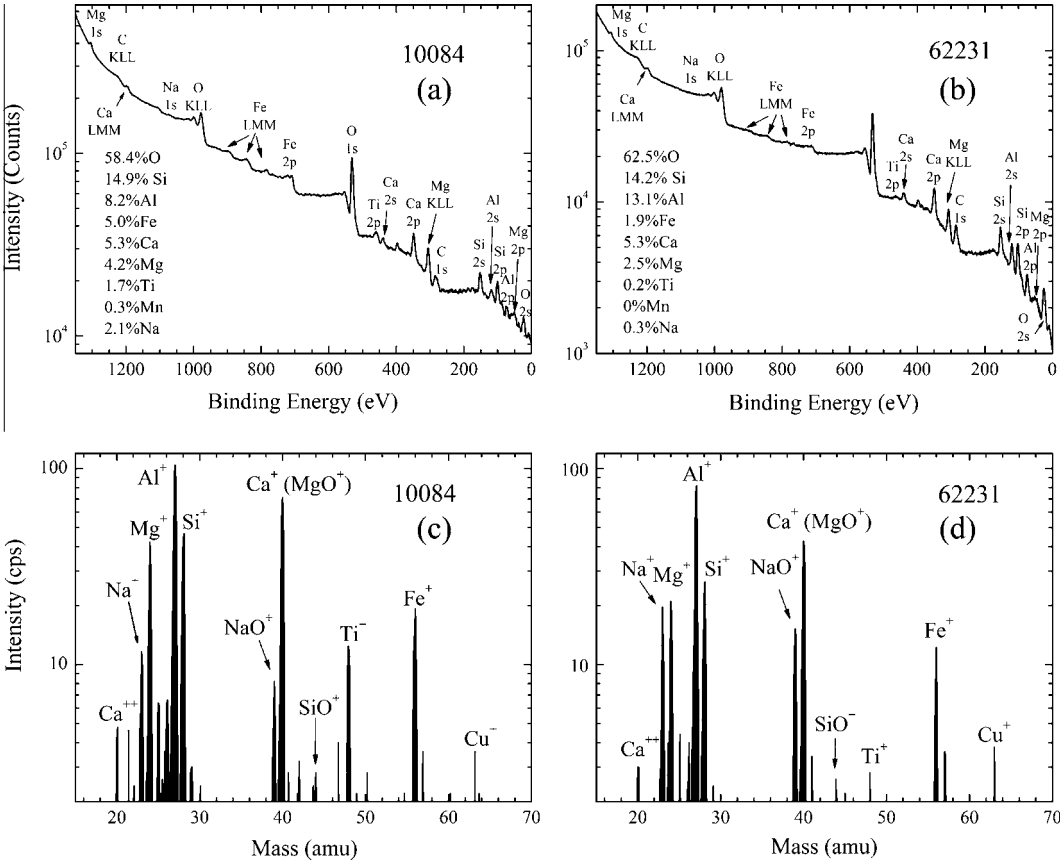

Fig. 4. (a) The Al Kα XPS spectrum and derived surface composition of mature lunar mare soil 10084 determined after SIMS measurements. (c) Secondary ion mass spectra of 10 eV ions ejected from the identical surface by 4 keV He^+. (b) and (d) Same as (a) and (c) but for lunar highland soil 62231. Cu^+ is likely an artifact derived from the Cu sample mount, and not intrinsic to the soil.

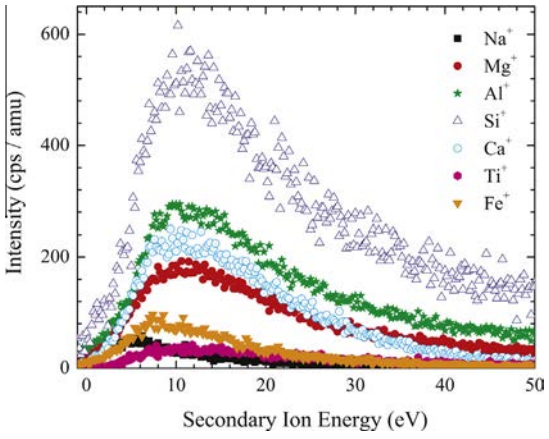

Fig. 5. Energy spectra of secondary ion ejected from mature lunar mare soil 10084 by 4 keV He^+ for different species.

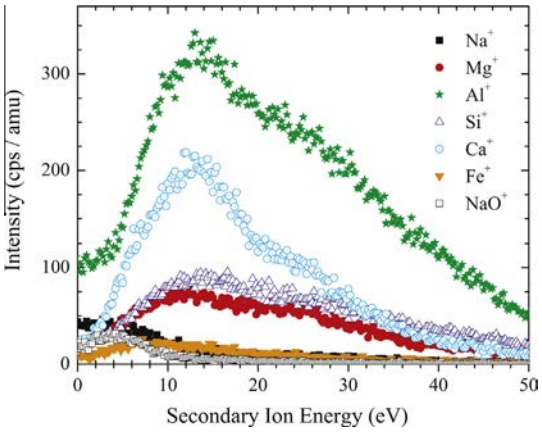

Fig. 6. Energy spectra of secondary ions ejected from mature lunar mare soil 62231 by 4 keV He^+ for different species.

vapor deposition by meteoritic impact, sputter redeposition, ion implantation, and preferential sputter removal. Since no enrichment in Ca or Mg is observed by Keller and McKay (1997), this data supports the conclusion that ion irradiation alone is insufficient to produce the lunar grain rims.

The secondary ion mass spectra ejected by 4 keV He generally match the atomic composition of the lunar surface, with enhanced alkali and alkaline metal (Na^+, Mg^+, Ca^+, Ca^{++}) content due to the lower surface binding energy of these atoms and low ionization potential (Fig. 4) (Kudriavtsev et al., 2004; Johnson and Baragiola, 1991). Ions derived from soil 62231 show strong Na^+, matching the greater feldspathic content of the highland soil (Fig. 4d). Ti^+ is primarily observed in 10084, reflecting the higher concentration of ilmenite in the lunar mare (Fig. 4c). These results are qualitatively similar to secondary ion spectra measured on lunar soil simulants by Elphic et al. (1991), measured with 1.5 keV protons, 4 keV He^+, and 5 keV Ar^+ and Ne^+. We note that the relative yields vary significantly with secondary ion energy. This is not unexpected, based on the measured secondary ion energy distributions (Figs. 5 and 6).

Table 2
SIMS conversion factors given by the ratio of relative ion yields to atomic percentage surface concentration for lunar soils (10084 and 62231) and JSC Corning glass lunar simulant.

Element	10084	62231	Corning glass
SIMS relative conversion factors			
Ca	0.23	0.26	0.19
Mg	0.30	0.22	0.18
Al	0.25	0.38	0.31
Si	1.02	1.14	1.09
Ti	0.33	0.19	0.45
Fe	0.80	0.40	0.72
Na	0.23	0.04	0.19

The sputtering yield, or the number of particles removed from a solid per incident primary ion, is largely a function of the surface concentration and binding energy of the atom to the surface, with a small dependence on mass and energy of the primary ion and the mass of the sputtered particle (Johnson and Baragiola, 1991). Secondary ion yields are dependent on the same parameters as neutral sputtering, with the additional dependence on the ionization probability for the atom as it leaves the solid. However, the absolute secondary ion yield is not easily measured, as this value is dependent on specific sample and experimental parameters as:

$$Y_s = \frac{I_s}{I_p \cdot (C \cdot F \cdot B \cdot \varepsilon_{Det})} \quad (1)$$

where I_s is the secondary ion count rate in the mass spectrometer for a particular species, I_p is the number of incident ions, C is the sample species atomic concentration, F is a factor which describes the isotopic and observed species fraction, B is the ionization probability, and ε_{Det} includes the spectrometer transmission and detection efficiency and varies inversely with mass. Since the matrix dependent ionization probability, spectrometer transmission, and detection efficiency are unknown, a quantitative species-specific ion sputtering yield cannot be directly determined from these measurements. Instead, we determine relative conversion factors (CF) to allow the correlation of secondary ion count rate to surface abundances.

For these measurements, we assume that the soils have been sputtered to equilibrium, so no correction for preferential sputtering is required. We derive conversion factors for 10 eV secondary ions based on the known surface atomic composition of the sample and the observed total secondary ion count rate for each species. The approximate lunar soil composition (in atomic percentage) can be obtained by dividing the number of detected secondary ions at each mass by the conversion factors given in Table 2 to provide a relative concentration for each species. These conversion factors are general and may be applied to any measurement using a mass spectrometer with a transmission inversely dependent on mass, including spaceflight instrumentation. The CF vary by less than 45% between lunar samples soils, except for Fe and Na. We note that remote surface compositions based on secondary ion abundance will be elemental in nature, averaged over an inhomogeneous regolith, and should not be used to infer mineralogy.

5. Conclusion

This study demonstrates that appreciable numbers of secondary ions ejected by solar wind type ions from lunar soils can be measured in minutes in the laboratory, and by extension observable on the Moon. While SIMS spectra presented here do not directly reproduce the lunar surface composition, the combination of laboratory SIMS and XPS data should enable the extraction of quantitative information about the surface from a spacecraft that measures exospheric ion abundances.

The secondary ion spectra measured in this study remain strongly representative of the lunar exospheric composition and suggest the existence of Na^+, Ca^{++}, Ca^+, Mg^+, Al^+, Si^+, Ti^+, and Fe^+, as well as molecular NaO^+, MgO^+, and SiO^+ in the lunar environment. We note that, although oxygen is sputtered from the surface (Meyer et al., 2011), O^+ ions are an insignificant fraction of the secondary ion spectrum.

Acknowledgments

The authors would like to thank R. Christoffersen and Doug Ming (microprobe analysis) for the preparation and loan of the Corning glass lunar simulant standard, and U. Raut and E. Mitchell for their comments on this manuscript. This work was supported through the NASA Cosmochemistry (NNX11AH19G) NSF Astronomy (AST-1413380), and the NASA LASER (NNX14AQ109) programs.

References

Baron, R.L., Bilson, E., Gold, T., Colton, R.J., Hapke, B., Steggert, M.A., 1977. The surface composition of lunar soil grains: A comparison of the results of Auger and X-ray photoelectron (ESCA) spectroscopy. Earth Planet. Sci. Lett. 37, 263–272.
Batey, J.H., 1987. Residual gas analysers. Vacuum 37 (8/9), 659–668.
Betz, G., Wehner, G.K., 1983. Sputtering of multicomponent materials. In: Behrisch, R. (Ed.), Sputtering by Particle Bombardment II. Springer-Verlag, Germany, p. 82.
Bjorkholm, P., Golub, L., Gorenstein, P., 1973. Detection of a nonuniform distribution of polonium-210 on the Moon with the Apollo 16 alpha particle spectrometer. Science 180 (4089), 957–959.
Dukes, C.A., Baragiola, R.A., McFadden, L.A., 1999. Surface modification of olivine by H^+ and He^+ bombardment. J. Geophys. Res. Planets 104 (E1), 1865–1872.
Dukes, C.A., Chang, W.-Y., Famá, M., Baragiola, R.A., 2011. Laboratory studies of the sputtering contribution to the sodium atmospheres of Mercury and the Moon. Icarus 212, 463–469.
Eick, M.J., Grossl, P.R., Golden, D.C., Sparks, D.L., Ming, D.W., 1996. Dissolution kinetics of a lunar glass simulant at 25 °C: The effect of pH and organic acids. Geochim. Cosmochim. Acta 60 (1), 157–170.
Elphic, R.C. et al., 1991. Lunar surface composition and solar wind-induced secondary ion mass spectrometry. Geophys. Rev. Lett. 18 (11), 2165–2168.
Feldman, P.D., Hurley, D.M., Retherford, K.D., Gladstone, G.R., Stern, S.A., Pryor, W., Parker, J.W., Kaufmann, D.E., Davis, M.W., Versteeg, M.H., 2012. Temporal variability of lunar exospheric helium during January 2012 from LRO/LAMP. Icarus 221 (2), 854–858.
Gorenstein, P., Bjorkholm, P., 1973. Detection of radon emanation from the crater Aristarchus by the Apollo 15 alpha particle spectrometer. Science 179 (4075), 792–794.
Hapke, B., 2001. Space weathering from Mercury to the asteroid belt. J. Geophys. Res. 106 (E5), 10039–10073.
Hilchenbach, M., Hovestadt, D., Klecker, B., Möebius, E., 1993. Observation of energetic lunar pick-up ions near Earth. Adv. Space Res. 13 (10), 321–324.
Hodges Jr., R.R., 1973. Helium and hydrogen in the lunar atmosphere. J. Geophys. Res. 78, 8055–8064.
Hoffman, J.H. et al., 1973. Lunar atmospheric composition results from Apollo 17. Geochim. Cosmochim. Acta 3, 2865–2875, Proc. Lunar Sci. Conf. 4.
Johnson, R.E., Baragiola, R.A., 1991. Lunar surface: Sputtering and secondary ion mass spectrometry. Geophys. Res. Lett. 18 (11), 2169–2172.
Keller, L.P., McKay, D.S., 1997. The nature and origin of lunar grain rims. Geochim. Cosmochim. Acta 61 (11), 2331–2341.
Korotev, R.L., 1981. Compositional trends in Apollo 16 soils. Proc. Lunar Sci. Conf. 12B, 577–605.
Korotev, R.L., 1982. Comparative geochemistry of Apollo 16 surface soils an samples from cores 64002 and 60002 thru 60007. Proc. Lunar Sci. Conf. 13, A269–A278.
Korotev, R.L., Gillies, J.J., 2001. A new look at the Apollo 11 regolith and KREEP. J. Geophys. Res. 106, 12339–12353.
Kudriavtsev, Y., Villegas, A., Godines, A., Asomoza, R., 2004. Calculation of the surface binding energy for ion sputtered particles. Appl. Surf. Sci. 239, 273–278.
Lawson, S.L. et al., 2005. Recent outgassing from the lunar surface: The Lunar Prospector alpha particle spectrometer. J. Geophys. Res. 110 (E9), E09009.
Loeffler, M.J., Dukes, C.A., Baragiola, R.A., 2008. Irradiation of olivine by 4 keV He^+: Simulation of space weathering by the solar wind. J. Geophys. Res. 114 (E03003), 1–13.
Magee, C.W., Harrington, W.L., 1978. Depth profiling of sodium in SiO_2 films by secondary ion mass spectrometry. Appl. Phys. Lett. 33 (2), 193–196.
Meyer, F.W., Harris, P.R., Taylor, C.N., Meyer III, H.M., Barghouty, A.F., Adams, J.H., 2011. Sputtering of lunar regolith simulant by protons and singly and multicharged Ar ions at solar wind energies. Nucl. Instrum. Meth. B 269, 1316–1320.

Poppe, A.R., Halekas, J.S., Sarantos, M., Delory, G.T., 2013. The self-sputtered contribution to the lunar exosphere. J. Geophys. Res. 118, 1–11.
Potter, A.E., Morgan, T.H., 1988. Discovery of sodium and potassium vapor in the atmosphere of the Moon. Science 241 (4866), 675–680.
Sheffer, A.A., 2007. Chemical Reduction of Silicates by Meteorite Impacts and Lightning Strikes. PhD Thesis, University of Arizona, ProQuest Information and Learning Company, Ann Arbor, MI, p. 43.
Stern, A., 1999. The lunar atmosphere: History, status, current problems, and context. Rev. Geophys. 37 (4), 453–491.
Stern, S.A., Retherford, K.D., Tsang, C.C.C., Feldman, P.D., Pryor, W., Gladstone, G.R., 2012. Lunar atmospheric helium detections by the LAMP UV spectrograph on the Lunar Reconnaissance Orbiter. Geophys. Res. Lett. 39 (12), L12202.
Stern, S.A., Cook, J.C., Chaufray, J.-Y., Feldman, P.D., Gladstone, G.R., Retherfornd, K.D., 2013. Lunar atmospheric H_2 detections by the LAMP UV spectrograph on the Lunar Reconnaissance Orbiter. Icarus 226 (2), 1210–1213.
Vorburger, A. et al., 2014. First direct observation of sputtered lunar oxygen. J. Geophys. Res.: Space 119 (2), 709–722.
Wagner, C.D., 1983. Sensitivity factors from XPS analysis of surface atoms. J. Electron. Spectrosc. Relat. Phenom. 32 (2), 99–102.
Yokota, S., Saito, Y., Asamura, K., Tanaka, T., Nishino, M.N., Tsunakawa, H., Shibuya, H., Matsushima, M., Shimizu, H., Takahashi, F., Fujimoto, M., Mukai, T., Terasawa, T., 2009. First direct detection of ions originating from the Moon by MAP-PACE IMA onboard SELENE (KAGUYA). Geophys. Res. Lett. 36, L11201.
Yokota, S., Tanaka, T., Saito, Y., Asamura, K., Nishino, M.N., Fujimoto, M., Tsunakawa, H., Shibuya, H., Matsushima, M., Shimizu, H., Takahashi, F., 2014. Structure of the ionized lunar sodium and potassium exosphere: Dawn-dusk asymmetry. J. Geophys. Res. Planets 119, 798–809.